Check for updates



NANO · MICRO small
www.small-journal.com

# Remotely Guided Immunobots Engaged in Anti-Tumorigenic Phenotypes for Targeted Cancer Immunotherapy

*Nihal Olcay Dogan, Hakan Ceylan,* Eylül Suadiye, Devin Sheehan, Asli Aydin, Immihan Ceren Yasa, Anna-Maria Wild, Gunther Richter, and Metin Sitti**

**Building medical microrobots from the body's own cells may circumvent the biocompatibility concern and hence presents more potential in clinical applications to improve the possibility of escaping from the host defense mechanism. More importantly, live cells can enable therapeutically relevant functions with significantly higher efficiency than synthetic systems. Here, live immune cell-derived microrobots from macrophages, i.e., *immunobots*, which can be remotely steered with externally applied magnetic fields and directed toward anti-tumorigenic (M1) phenotypes, are presented. Macrophages engulf the engineered *magnetic decoy bacteria*, composed of 0.5 μm diameter silica Janus particles with one side coated with anisotropic FePt magnetic nanofilm and the other side coated with bacterial lipopolysaccharide (LPS). This study demonstrates the torque-based surface rolling locomotion of the immunobots along assigned trajectories inside blood plasma, over a layer of endothelial cells, and under physiologically relevant flow rates. The immunobots secrete signature M1 cytokines, IL-12 p40, TNF-α, and IL-6, and M1 cell markers, CD80 and iNOS, via toll-like receptor 4 (TLR4)-mediated stimulation with bacterial LPS. The immunobots exhibit anticancer activity against urinary bladder cancer cells. This study further demonstrates such immunobots from freshly isolated primary bone marrow-derived macrophages since patient-derivable macrophages may have a strong clinical potential for future cell therapies in cancer.**

## 1. Introduction

Untethered mobile microrobots have significant potential to access hard-to-reach, deep, and risky human body regions for minimally invasive medical interventions.[1] So far, various mobile microrobotic platforms have been developed using versatile synthetic materials or self-propelled motile microorganisms (e.g., bacteria and microalgae) that have been further modified with functional units for a targeted medical application.[2] However, such synthetic and biohybrid microrobots cannot be long-term deployed in the body since they are typically deleterious and promptly cleared by the body's immune system,[3] where the failure may lead to the formation of granulomas and inflammation.[4] Our recent research has applied a new concept in the microrobotics field; a personalized medicine approach through patient-blood derivable biomaterials in the fabrication of microrobots to minimize safety risks and unintended immune responses.[5] Although the personalized microrobots we conceptualized can significantly reduce immunogenicity-related issues, regardless of the high proportions of patient materials we use, these microrobots still include additional synthetic components, such as magnetic nanoparticles and photoinitiators, which may still be recognized by the immune system. Hence, untethered medical microrobots still require considerable improvements before being used in clinics.

N. O. Dogan, H. Ceylan, D. Sheehan, A. Aydin, I. C. Yasa, A.-M. Wild, M. Sitti
Physical Intelligence Department
Max Planck Institute for Intelligent Systems
70569 Stuttgart, Germany
E-mail: ceylan.hakan@mayo.edu; sitti@is.mpg.de

N. O. Dogan, M. Sitti
Institute for Biomedical Engineering
ETH Zurich
Zurich 8092, Switzerland

H. Ceylan
Department of Physiology and Biomedical Engineering
Mayo Clinic
Scottsdale, AZ 85259, USA

E. Suadiye, G. Richter
Materials Central Scientific Facility
Max Planck Institute for Intelligent Systems
70569 Stuttgart, Germany

M. Sitti
School of Medicine and College of Engineering
Koç University
Istanbul 34450, Turkey

The ORCID identification number(s) for the author(s) of this article can be found under https://doi.org/10.1002/smll.202204016.

© 2022 The Authors. Small published by Wiley-VCH GmbH. This is an open access article under the terms of the Creative Commons Attribution License, which permits use, distribution and reproduction in any medium, provided the original work is properly cited.

**DOI: 10.1002/smll.202204016**

16136829, 2022, 46, Downloaded from https://onlinelibrary.wiley.com/doi/10.1002/smll.202204016 by Koc University, Wiley Online Library on [15/04/2023]. See the Terms and Conditions (https://onlinelibrary.wiley.com/terms-and-conditions) on Wiley Online Library for rules of use; OA articles are governed by the applicable Creative Commons License

As a potential alternative to fully synthetic or biohybrid microrobots, building medical microrobots from living cells that could be harvested from the human body has more potential in clinical applications since the body would recognize them as self when infused back.[6] More importantly, living cell-based therapies can perform sustainable long-term therapeutic functions that conventional drugs and biologics cannot.[7] Among various cell types, immune cells have significant attention due to their natural abilities, such as defending the body from foreign intruders and tumors. Lymphocyte-based therapies are more widespread; however, their efficacy in treating solid tumors remains elusive due to reduced penetration of lymphocytes into dense fibrotic tumor tissue. Unlike lymphocyte-based therapies, macrophages are more promising candidates for treating solid tumors due to their active accumulation and penetration into the dense tumor tissue microenvironment. Furthermore, while lymphocytes offer tumoricidal activities upon direct contact with tumor cells, macrophages combine direct tumor-killing with indirect killing using the ability to recruit endogenous immunity via cytokine secretion and antigen presentation.[8] Hence, macrophages have recently paved the way to elicit new treatments for solid tumors.

Macrophages are tremendously plastic cell types capable of shifting their phenotypes depending on environmental cues.[9] In the case of cancer, macrophages can often be in two main phenotypes guiding their polarization in response to environmental stimuli, classically activated pro-inflammatory (M1) and alternatively activated anti-inflammatory (M2) macrophages.[10] M1 macrophages secrete pro-inflammatory cytokines (i.e., interleukin 12 (IL-12), tumor necrosis factor-alpha (TNF-$\alpha$), interleukin-6 (IL-6)) to the surrounding microenvironment and express specific cell markers (i.e., cluster of differentiation 80 (CD80), inducible nitric oxide synthase (iNOS)) that promote and exhibit enhanced tumoricidal activity.[11] On the other hand, M2 macrophages promote tumor growth by introducing an immunosuppressive tumor microenvironment through the production of different cytokines and markers (i.e., interleukin-10 (IL-10) and arginase-1 (Arg-1)), ultimately leading to tumor angiogenesis, invasion, and metastasis.[12] Hence, a central goal of macrophage-based therapies in cancer immunotherapy is maintaining anti-tumorigenic M1 macrophages and reducing the proportion of M2 macrophages.

Macrophages could turn their polarization into M1 phenotypes upon recognition of pathogen-associated molecular patterns. Lipopolysaccharide (LPS) is a pathogen-associated molecular pattern found abundantly on the cell wall of gram-negative bacteria that stimulates macrophages through the interaction with toll-like receptor 4 (TLR4).[13]

Here, we report macrophage-based microrobots, bringing together robotic mobility control and immunomodulatory functions for the first time: i) stimulating and sustaining macrophages towards the anti-tumorigenic (M1) phenotypes and ii) controlling their direction of motion precisely using an external magnetic field. For this purpose, we first presented engineered *magnetic decoy bacteria*, which compromised two functional units; FePt film coating and bacterial LPS. Macrophages have a natural phagocytosis capability where the cells recognize and internalize foreign materials to protect the body from foreign substances and pathogens.[14] Using the inherent phagocytosis properties, we constructed *immunobots* composed of living macrophages encapsulated magnetic decoy bacteria with a high yield production process (≈99.2%). The magnetic decoy bacteria strategy developed here enabled us to regulate macrophages': i) phenotypes toward the anti-tumorigenic state due to TLR4-mediated stimulation of macrophages with the bacterial LPS and (ii) steerable surface rolling due to the hard magnetic FePt film. The M1 activation state of immunobots was proved by measuring M1/M2 cytokines secretion; (i.e., IL-12, TNF-$\alpha$, IL-6, and IL-10) and M1/M2 markers expression (i.e., CD80, iNOS, and Arg-1). The conditioned medium harvested from immunobots significantly inhibited the mouse urinary bladder cancer cell growth in vitro, where the viability of cancer cells was reduced to 14%. Moreover, we demonstrated that such immunobots could be constructed from freshly isolated primary bone marrow-derived macrophages, which have remarkable clinical potential since patient-derivable autologous biomaterials are the safest option to avoid unwanted immune reactions in the body and have the potential to inspire the design of various future medical robots and interventional devices for their improved biocompatibility.

## 2. Results and Discussion

### 2.1. Concept of Immunobots

We used a particle-based strategy, where 0.5 µm-diameter silica particles compromised two components: FePt hard magnetic film and bacterial LPS stimulator (**Figure 1**A). We used the FePt film for its convenient properties, including high coercivity, chemical stability, and biocompatibility.[15] We performed the thin FePt coating (60 nm thickness) using a molecular epitaxy system described previously.[15a] Since the particle size was slightly different compared to the previous design, we confirmed the uniform coating of the FePt layer (60 nm thickness) around half of the silica particles with images acquired by scanning electron microscopy (SEM) and transmission electron microscopy (TEM) (Figure S1, Supporting Information). The half coating with FePt was required to provide shape anisotropy, allowing efficient and robust control of microparticles' orientation and velocity.[16] The magnetic properties of FePt-coated silica particles were also investigated using a vibrating sample magnetometer (VSM), where the coercivity of the FePt-coated particles was measured as 875 mT (Figure S2, Supporting Information). After ensuring the uniform FePt coating, we further modified silica particles' uncoated sides with bacterial LPS through a consecutive series of chemical reactions. The conjugation of particles with bacterial LPS enabled us to achieve phenotypic control over macrophages. The resultant magnetic decoy bacteria were detectable under fluorescence microscopy through the conjugation of FITC-labeled streptavidin (Figure S3, Supporting Information).

As a next step, macrophages were cultured in a cell culture medium containing magnetic decoy bacteria. The phagocytosis of magnetic decoy bacteria by macrophages led to magnetically controllable anti-tumorigenic immunobots, where the cells could produce pro-inflammatory (M1) cytokines to initiate an immune response (Figure 1B). The secretion of these


© 2022 The Authors. Small published by Wiley-VCH GmbH

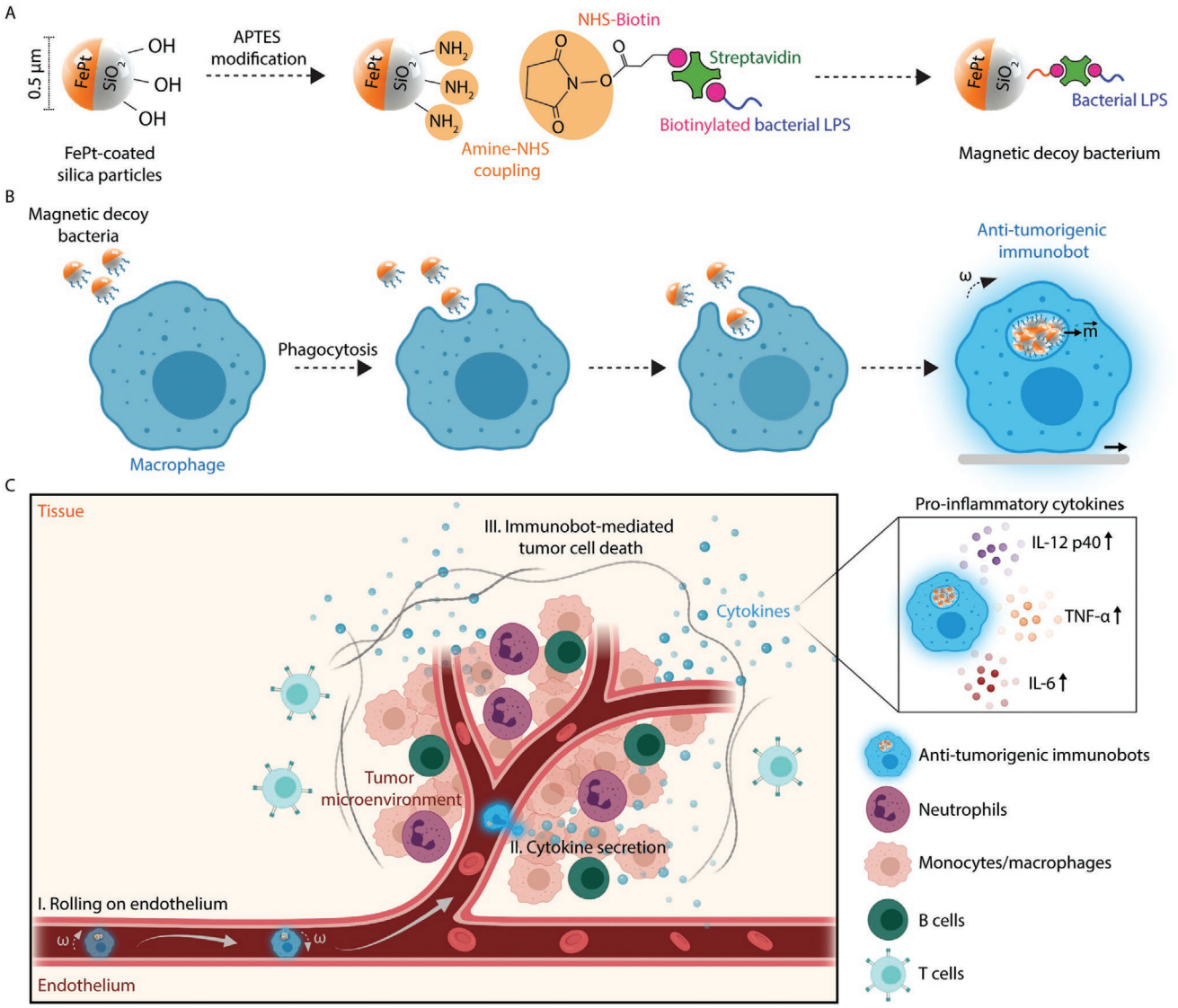



**Figure 1.** Our envisioned strategy of immunobots in cancer immunotherapy. A) A magnetic decoy bacterium comprises a silica core half-coated with FePt, further conjugated with bacterial LPS. B) The internalization of magnetic decoy bacteria by macrophages through their inherent phagocytosis process leads to immunobots in which the navigation direction of cells' could be precisely controlled due to the FePt layer, and anti-tumorigenic phenotypes could be maintained in a sustainable manner due to the bacterial LPS. C) A conceptual schematic depicts wireless rolling and steering control of immunobots on an endothelial layer towards a tumor microenvironment to recruit surrounding host immune cells to the targeted area through cytokine secretion for targeted cancer immunotherapy.

pro-inflammatory cytokines could activate other host immune cells, improve lymphocytes' infiltration to the tumor site, inhibit immunosuppressive cells in that microenvironment, and contribute to antitumor immunity (Figure 1C).

### 2.2. Preparation and Characterization of Immunobots

Macrophages were tracked in real time during the phagocytosis process, sensing the magnetic decoy bacteria in a short duration and crawling along the surface to internalize and eliminate them. Even within 15 min of incubation, macrophages phagocytosed the first batch of magnetic decoy bacteria by wrapping their cell membrane around them and continued to internalize the surrounding ones (**Figure 2**A and Movie S1, Supporting Information). However, we routinely incubated macrophages with the magnetic decoy bacteria overnight to provide sufficient time for the cells to encapsulate the maximum amount of particles. In the following experiments of this paper, the term *immunobots* refer to macrophages incubated with the magnetic decoy bacteria consistently overnight.

We first evaluated the immunobots using SEM, where we observed that a single macrophage could simultaneously interact with multiple magnetic decoy bacteria (Figure S4, Supporting Information). However, SEM imaging provides information exclusively about surface topology. To ensure that the macrophages fully internalized the magnetic decoy bacteria, we fluorescently stained the compartments of the macrophages, their nuclei, and their actin filaments. After overnight


© 2022 The Authors. Small published by Wiley-VCH GmbH

16136829, 2022, 46, Downloaded from https://onlinelibrary.wiley.com/doi/10.1002/smll.202204016 by Koc University, Wiley Online Library on [15/04/2023]. See the Terms and Conditions (https://onlinelibrary.wiley.com/terms-and-conditions) on Wiley Online Library for rules of use; OA articles are governed by the applicable Creative Commons License

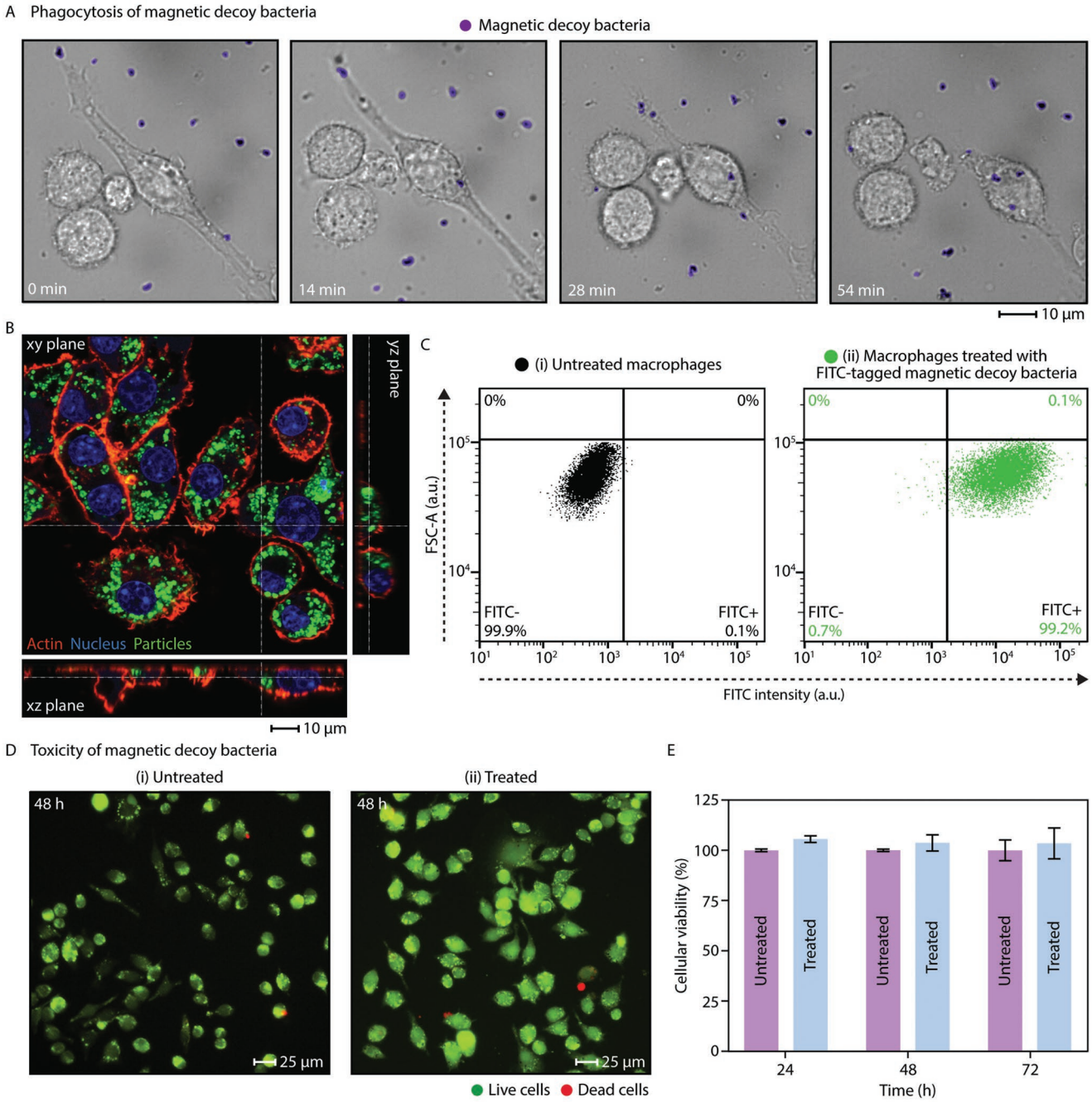



**Figure 2.** Preparation and characterization of immunobots. A) Time-lapse differential interference contrast (DIC) images of macrophages phagocytosing magnetic decoy bacteria. The magnetic decoy bacteria were pseudocolored. B) Confocal z-stack images demonstrated macrophages with fully internalized magnetic decoy bacteria. C) Flow cytometry density plots of i) bare macrophages and ii) macrophages treated with FITC-tagged magnetic decoy bacteria indicated that 99.2% of macrophages engulfed magnetic decoy bacteria after overnight incubation (a.u.: arbitrary unit, $n = 10\,000$ events per group). D,E) Assessing the biocompatibility of magnetic decoy bacteria with macrophages. D) Representative fluorescence images of the macrophages stained with calcein-AM/ethidium homodimer-1 after 48 h of exposure to magnetic decoy bacteria. E) The percentage of viable macrophages after exposure to magnetic decoy bacteria for different periods was assessed based on the quantified intracellular adenosine 5′-triphosphate (ATP) amount using the CellTiter-Glo assay. Data were presented as mean ± SD, $n = 3$.

incubation, fluorescently detectable magnetic decoy bacteria were revealed at the inner borders of the macrophages by 3D reconstruction of the Z-stacks (Figure 2B).

Next, we calculated the encapsulation efficiency of the macrophages during immunobot production. For the characterization, we used two groups: i) untreated macrophages and ii) macrophages treated with FITC-tagged magnetic decoy bacteria overnight. A gate was first created using the untreated macrophages, and this gate was further used for the treated group. The flow cytometry density plots indicated that 99.2% of the


© 2022 The Authors. Small published by Wiley-VCH GmbH

16136829, 2022, 46, Downloaded from https://onlinelibrary.wiley.com/doi/10.1002/smll.202204016 by Koc University, Wiley Online Library on [15/04/2023]. See the Terms and Conditions (https://onlinelibrary.wiley.com/terms-and-conditions) on Wiley Online Library for rules of use; OA articles are governed by the applicable Creative Commons License

macrophages internalized the magnetic decoy bacteria after overnight incubation (Figure 2C), resulting in a high-yield production process.

Furthermore, we evaluated the biocompatibility of the magnetic decoy bacteria with the macrophages depending on two methodologies: i) membrane integrity measurements with live/dead (Calcein-AM/Ethidium homodimer-1) staining and ii) metabolic activity measurements with intracellular adenosine-5′-triphosphate (ATP) quantification using CellTiter-Glo cell viability assay. We treated mouse peritoneal macrophage cells, J774A.1, with the magnetic decoy bacteria for different periods. Calcein-AM and ethidium homodimer-1 were the molecules used in the membrane integrity measurements. Calcein-AM is a non-fluorescent molecule that can be permeabilized through the cell membrane. Once calcein-AM enters the cell, it is converted into a fluorescent form, calcein, upon hydrolysis of lipophilic groups by intracellular esterases in living cells.[17] Calcein becomes trapped in the cytoplasm of live cells and could be detected under fluorescent microscopy (Ex/Em: 488/520 nm). In contrast, ethidium homodimer-1 is a molecule with a strong positive charge that prevents its passage through the cell membrane of living cells. In the case of cells with ruptured membranes, ethidium homodimer-1 penetrates the cell, binds to the DNA, and gives a fluorescent signal (Ex/Em: 528/617 nm). Here, membrane integrity measurements revealed that immunobots still had intact plasma membranes even after 72 h of incubation, including a small proportion of dead cells of the total cell population (Figure 2D and Figure S5, Supporting Information).

Although membrane integrity assessment is a certain way to prove cell viability, it does not provide evidence of cell proliferation. Instead, measuring the metabolic activities of cells provides information on cell proliferation since ATP amounts of the treated cells were compared with the untreated cells undergoing a normal cell division process. The metabolic activity measurements indicated that immunobots demonstrated similar proliferation rates compared to the untreated macrophages (Figure 2E). In conclusion, biocompatibility analyses indicated that the macrophages did not exhibit an acute toxic response against the magnetic decoy bacteria within the given time frame.

### 2.3. Magnetic Actuation and Steering of Immunobots

Magnetic control of cell-based robots using external permanent magnets has been demonstrated. However, these systems have many drawbacks in experimental repeatability, positional accuracy, and steering precision. In these previous studies, magnet movement largely depends on manual handling, and its magnitude could not be changed in a short duration restrains the precise position control of cell-based microrobots.[18] Even when permanent magnets are robotically controlled, the gradient pulling results in jerky body motions. To overcome these drawbacks, we used a custom-made Helmholtz electromagnetic coil setup mounted on an inverted optical microscope, where the five-coiled electromagnetic setup system enabled precise surface rolling locomotion and steering of immunobots along a predefined trajectory compared to those that utilized magnetic gradient-based pulling.

The electromagnetic setup we used here can generate a uniform external rotating magnetic field in the range of 1–20 mT in the given workspace. The uniform rotating magnetic fields are applied to exert magnetic torque to rotate the immunobots. As the FePt carries magnetic anisotropy for being in the half sphere shape, its easy axis tends to align with the external field. Internalization of the Janus particles into the cell phagosomes ensures that the particles remain fixed in the cell and are not free to rotate. Thus, the externally applied magnetic fields are converted into torques that rotate the cell on the surface and drive the rolling locomotion. By changing the rotational magnetic field's orientation, we could precisely control the direction of the immunobots' surface rolling locomotion.

First, we demonstrated that the immunobots could be rolled and steered along the desired trajectories on a glass surface, where the cells were either suspended in a cell culture medium or more physiologically relevant fluid, inside blood plasma (Movie S2, and Movie S3, Supporting Information). Until a critical threshold (step-out frequency), immunobots' translation speed is almost linearly proportional to the applied magnetic field frequency. Once this threshold is reached, the rotation speed is no longer linearly proportional to the rotation frequency, and the immunobots could no longer overcome the resistive torque exerted by the fluid, resulting in a rapid velocity decrease.[15b,19] Here, we also measured the step-out frequency and corresponding maximum mean velocities of immunobots by gradually increasing the rotational frequency of the magnetic field. The step-out frequency under 10 mT field strength was measured at 30 Hz with a maximum mean velocity of 82.2 $\mu m\ s^{-1}$ (**Figure 3**A). Step-out frequency is related to the number of magnetic decoy bacteria internalized by the cell, which means the maximum mean speed could be enhanced by increasing the concentration of the magnetic decoy bacteria incubated with the macrophages.

Next, we investigated the magnetic actuation and steering capabilities of immunobots on human umbilical vein endothelial cells (HUVECs) that constitute the inner lining of blood vessels.[20] We demonstrated that immunobots could locomote on heterogeneous biological topographies along desired trajectories in vitro (Figure 3B and Movie S4, Supporting Information). Thus, the immunobots could be magnetically actuated, steered on endothelial cells, and localized in a targeted tumor microenvironment in vivo.

Any microrobots administrated into the bloodstream should be steered along the blood flow and moved against it for controlled navigation and targeting. To demonstrate the rolling locomotion of immunobots in physiologically relevant flow conditions, we tested the motion of immunobots within a microfluidic channel mimicking the flow rates of venules and capillaries, 3 and 1 mm $s^{-1}$, respectively.[1b] Application of a rotating magnetic field at 10 mT and 30 Hz, the immunobots could be reliably steered against the flow at a 2 mm $s^{-1}$ flow rate (Movie S5, Supporting Information). At 4 mm $s^{-1}$ flow rates, fluidic drag on the immunobots began to balance the magnetic torque, resulting in a step out, and no net displacement was observed. Therefore, rolling is a reliable mode of locomotion in vivo. The circulatory system in the body consists of different forms of vessels that vary in dimensions and flow properties.[6a] To improve the remote steering performance of the immunobot rollers, e.g.,


© 2022 The Authors. Small published by Wiley-VCH GmbH

16136829, 2022, 46, Downloaded from https://onlinelibrary.wiley.com/doi/10.1002/smll.202204016 by Koc University, Wiley Online Library on [15/04/2023]. See the Terms and Conditions (https://onlinelibrary.wiley.com/terms-and-conditions) on Wiley Online Library for rules of use; OA articles are governed by the applicable Creative Commons License

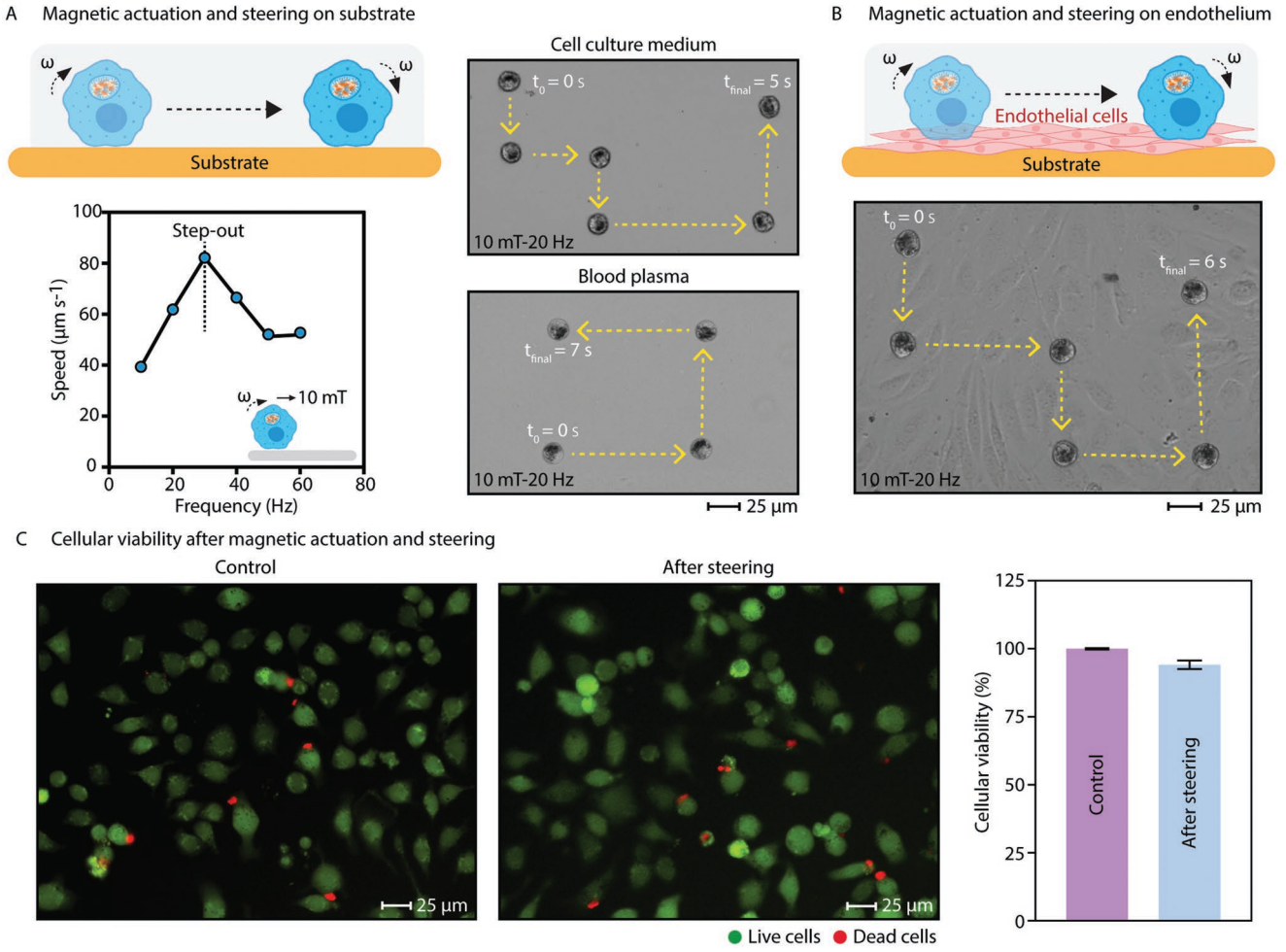



**Figure 3.** Magnetic torque-based surface rolling and steering of immunobots. A) Immunobots were capable of following predefined trajectories in cell culture medium and blood plasma on a glass substrate. The step-out frequency of immunobots in the cell culture medium under a 10 mT rotating magnetic field was determined as 30 Hz with a maximum mean speed of 82.2 µm s$^{-1}$ by increasing the rotation frequency of the magnetic field stepwise. B) Magnetic rolling and steering of immunobots on endothelial cells in vitro. C) The cellular viability of immunobots was assessed using calcein-AM/ethidium homodimer-1-staining after magnetic actuation and steering at 30 Hz under a 10 mT rotating magnetic field for 5 min. The immunobots were further collected and incubated overnight in a humidified chamber at 37 °C and 5% $CO_2$. The percentage of viable cells was evaluated after overnight incubation based on live and dead cell counting. Data were presented as mean ± SD, $n = 3$.

arteries, with a flow rate on the order of 10 cm s$^{-1}$, we need to improve the magnetization of cells. Our next development step will include depositing more layers of FePt on the Janus particles and increasing the actuating field strength and frequency.

Once the immunobots reach their target tissue, they must remain viable and perform their therapeutic function of secreting pro-inflammatory cytokines to recruit the host immune cells to the tumor microenvironment to stop the uncontrollable tumor cell growth. Thus, it is crucial to demonstrate the viability of immunobots after their active navigation to the target site. First, we steered the immunobots under a 10 mT rotating magnetic field at 30 Hz frequency for 5 min since the immunobots reached their maximum speed under these conditions (Figure 3A). Then, we collected the immunobots back and incubated them overnight in a humidified 37 °C and 5% $CO_2$ atmosphere. We found that the immunobots were still alive after magnetic actuation and steering, so they could still perform their anti-tumorigenic functions (Figure 3C).

### 2.4. Characterizing the Anti-Tumorigenic Activation States of Immunobots

Our magnetic decoy bacteria design used bacterial LPS as a potent activator, stimulating immunobots and switching their phenotypes into M1, which means the cells can detect and fight against tumors.[21] To prove that the stimulation of macrophages occurred through bacterial LPS, we performed experiments using different types of silica particles: i) coated simply with FePt, called LPS-free particles, and ii) magnetic decoy bacteria. We confirmed the anti-tumorigenic states of the immunobots by combining different strategies, quantifying cytokine secretion, and measuring the cell marker expression (**Figure 4**A). All characterizations were carried out on the following groups: i) bare macrophages, ii) macrophages treated with LPS-free particles, and iii) immunobots, where the cells were treated with magnetic decoy bacteria.


© 2022 The Authors. Small published by Wiley-VCH GmbH

16136829, 2022, 46, Downloaded from https://onlinelibrary.wiley.com/doi/10.1002/smll.202204016 by Koc University, Wiley Online Library on [15/04/2023]. See the Terms and Conditions (https://onlinelibrary.wiley.com/terms-and-conditions) on Wiley Online Library for rules of use; OA articles are governed by the applicable Creative Commons License

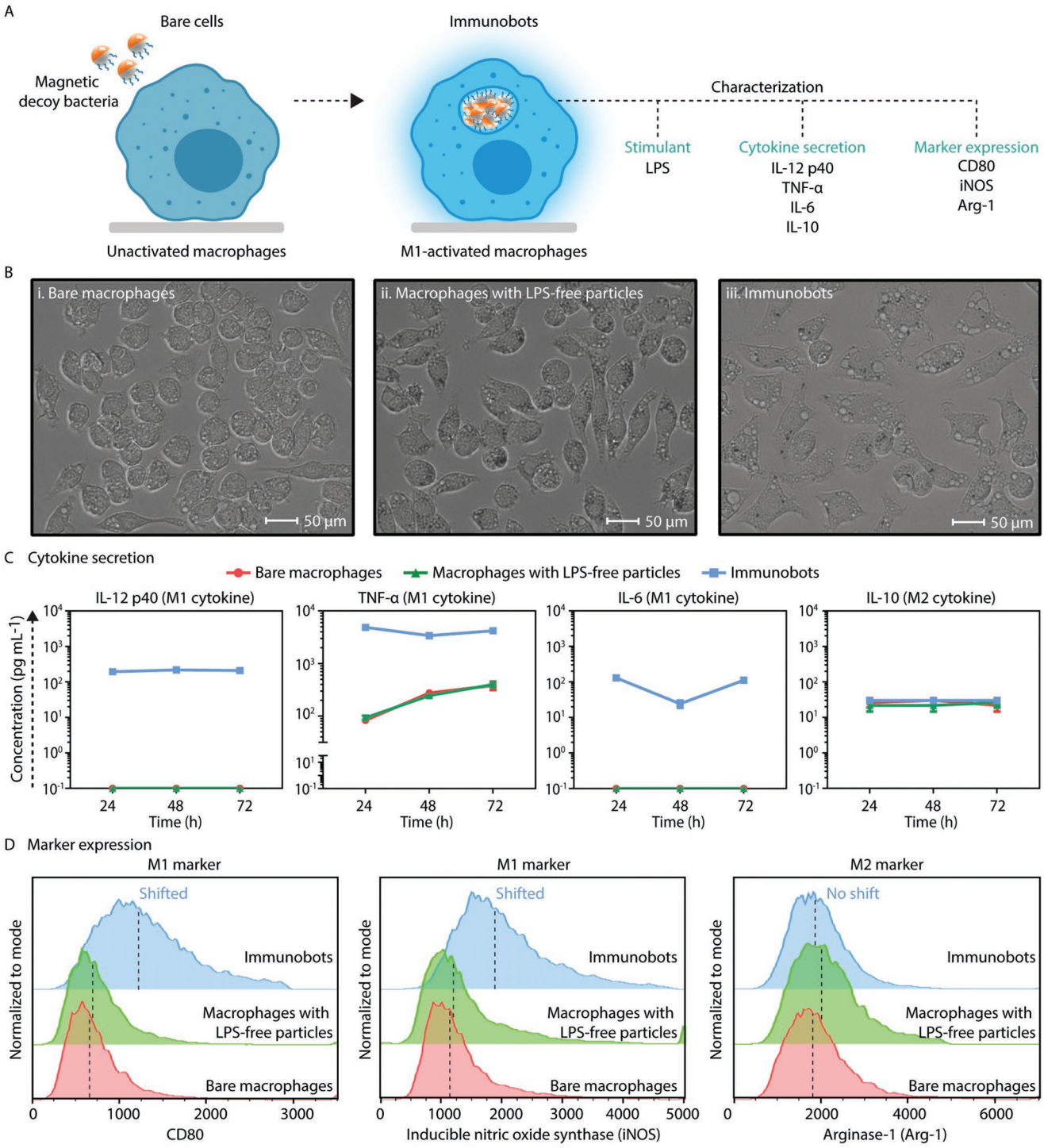



**Figure 4.** Regulating and sustaining phenotypes of macrophages toward an anti-tumorigenic state. A) The summary for modulating the phenotypes of macrophages. The stimulation of macrophages with bacterial LPS unit of magnetic decoy bacteria activated the release of specific cytokines and enhanced the expression levels of cell markers. B) Optical microscope DIC images of i) bare macrophages, ii) macrophages treated with LPS-free particles, and iii) immunobots. Incubation with magnetic decoy bacteria overnight increased cell size and resulted in distinct morphological changes. C) Analysis of macrophages' phenotypic states was performed by measuring the levels of M1 cytokines (IL-12 p40, TNF-$\alpha$, and IL-6) and M2 cytokines (IL-10). The immunobot group produced higher amounts of M1 cytokines compared to bare macrophages and macrophages treated with LPS-free particles, whereas the M2 cytokine was secreted at the same level for all groups. D) The expressions of M1 markers (CD80 and iNOS) and M2 marker (Arg-1) on macrophages were determined by flow cytometry ($n = 10\,000$ events per data point). The presence of bacterial LPS in the case of immunobots triggered higher expression of M1 markers without showing any significant change in M2 marker expression.


© 2022 The Authors. Small published by Wiley-VCH GmbH

16136829, 2022, 46, Downloaded from https://onlinelibrary.wiley.com/doi/10.1002/smll.202204016 by Koc University, Wiley Online Library on [15/04/2023]. See the Terms and Conditions (https://onlinelibrary.wiley.com/terms-and-conditions) on Wiley Online Library for rules of use; OA articles are governed by the applicable Creative Commons License

Nuclear and cytoplasmic morphological changes provide essential information for understanding cell differentiation and functions.[22] Hence, we first analyzed the morphologies of macrophages found in different treatment conditions. The imaging results exhibited that bare macrophages and macrophages with LPS-free particles had similar sizes and morphologies. In contrast, immunobots exhibited distinct morphological changes, including increase in cell size and granularity (Figure 4B).

Depending on their activation states, macrophages secrete signature cytokines, which leads to a pronounced change in cell function. M1-state macrophages secrete high levels of pro-inflammatory cytokines, mainly IL-12, TNF-$\alpha$, and IL-6, so their activation states can be identified based on measuring the secretion amounts of these cytokines.[23] Each M1 cytokine plays a crucial role in cancer treatment. For instance, TNF-$\alpha$ induces the apoptosis of certain tumor cells by enhancing the permeability of blood vessels so that the immune cells can easily infiltrate from the bloodstream to the tumor site.[24] IL-12 is essential to fight against tumors by activating and proliferating natural killer (NK) and T cells.[25] Ultimately, IL-6 promotes the proliferation and trafficking of lymphocytes to the tumor sites, where they can inhibit tumor growth and progression.[26] Conversely, M2-state macrophages can be characterized by high levels of IL-10, which plays an important role in tumor progression by suppressing cytotoxic NK and $CD8^+$ T cells.[27] Here, we characterized the activation states of the immunobots by comparing the secreted amounts of M1 and M2 cytokines, including IL-12 p40, a subunit of IL-12, TNF-$\alpha$, IL-6, and IL-10. The results indicated a significant increase in the M1 cytokines, whereas the M2 cytokine was at the same level for all groups after 72 h (Figure 4C). Moreover, we observed that LPS-free particles did not trigger any M1 cytokine secretion by the macrophages. Only in the case of engulfed magnetic decoy bacteria, immunobots were capable of secreting the M1 cytokines. Bacterial LPS, firmly bound on the surface of silica particles via biotin-streptavidin binding, achieved regulating and sustaining the M1 state of the immunobots.

Alternatively, macrophages express specific cell markers helpful in identifying their activation states. In addition to M1 cytokine secretion, we further proved the anti-tumorigenic states of the immunobots by evaluating the expression of specific cell markers, including CD80, iNOS, and Arg-1. CD80 and inducible nitric oxide synthase (iNOS) are key components showing the M1 activation states of macrophages. CD80 triggers inflammation and tissue damage, and iNOS initiates tumor cell apoptosis due to nitric oxide production.[28] Conversely, an increase in Arg-1 expression depicts M2 macrophages, contributing to tumor progression.[29] Here, we observed that immunobots showed higher expression in M1 markers, whereas there were no significant differences in M2 marker expression for all groups (Figure 4D). To conclude, the immunobots were able to express M1 cytokines/markers after 72 h in the absence of a tumor-suppressive microenvironment.

### 2.5. Antitumor Activity of Immunobots

The M1-state macrophages have two molecular mechanisms to kill cancer cells: (i) direct killing through the release of harmful products, including TNF-$\alpha$, nitric oxide (NO), and reactive oxygen species (ROS), and ii) indirect killing by recruiting surrounding host immune cells to the tumor area via pro-inflammatory cytokines secretion and antigen presentation, where the other host immune cells can kill cancer.[30] Here, we analyzed the antitumor activity of immunobots by investigating the direct killing molecular mechanism.

To investigate the antitumor activity of immunobots, we applied the conditioned medium approach, in which the cell culture medium containing the components secreted by cells is harvested and transferred to another set of cells for further analysis.[31] Here, we collected cell culture medium from i) bare macrophages, ii) macrophages treated with LPS-free particles, and ii) immunobots at 24 h of incubation. After treating mouse urinary bladder cancer cells with different media for 24 h, the cellular viabilities of cancer cells were analyzed depending on membrane integrity and metabolic activity measurements (**Figure 5**A). We observed that the media collected from i) bare macrophages and ii) macrophages treated with LPS-free particles did not trigger any cancer cell death since macrophages were unactivated in these control groups (Figure 4C,D). On the other hand, exposure of mouse urinary bladder cancer cells to the M1-activated immunobots conditioned medium suppressed the cancer cells' growth significantly, where the viability of cancer cells was reduced to 14% at 24 h of incubation (Figure 5B,C).

### 2.6. Construction of the Immunobots from Primary Macrophages

An alternative strategy to improve our immunobot design would be to implement a personalized medicine approach, where macrophages could be harvested from the patients themselves, expanded and engineered in the lab, and infused back into the patient. Immunobots made from patient-derivable autologous cells could minimize any risks of long-term cytotoxicity and improve the efficacy of cell-based robots since the body would recognize these engineered cells as its own.[5] Thus, personalized immunobots relying on freshly isolated primary macrophages from the body have more significant potential in clinical applications.

Here, we indicated that the immunobots could be fabricated using freshly isolated primary macrophages. For this purpose, bone marrow specimens were taken from mice to extract the precursor cells. To trigger the differentiation of the precursor cells into macrophages, we used the macrophage colony-stimulating factor (M-CSF) (**Figure 6**A). M-CSF is a growth factor that initiates a receptor-mediated intracellular signaling pathway and leads to the proliferation and differentiation of progenitors into macrophages.[32] Incubation for 6 d with M-CSF resulted in distinct morphological changes in the precursor cells (Figure 6B and Figure S6, Supporting Information). Progenitor cells in suspension started to adhere to the culture plate surface and differentiated into macrophages during 6 d of incubation with M-CSF. We analyzed the expression of CD11b and F4/80 markers to measure the number of progenitor cells differentiated into macrophages. These are unique markers of macrophages: CD11b plays a critical role in antigen clearance,


© 2022 The Authors. Small published by Wiley-VCH GmbH

16136829, 2022, 46, Downloaded from https://onlinelibrary.wiley.com/doi/10.1002/smll.202204016 by Koc University, Wiley Online Library on [15/04/2023]. See the Terms and Conditions (https://onlinelibrary.wiley.com/terms-and-conditions) on Wiley Online Library for rules of use; OA articles are governed by the applicable Creative Commons License

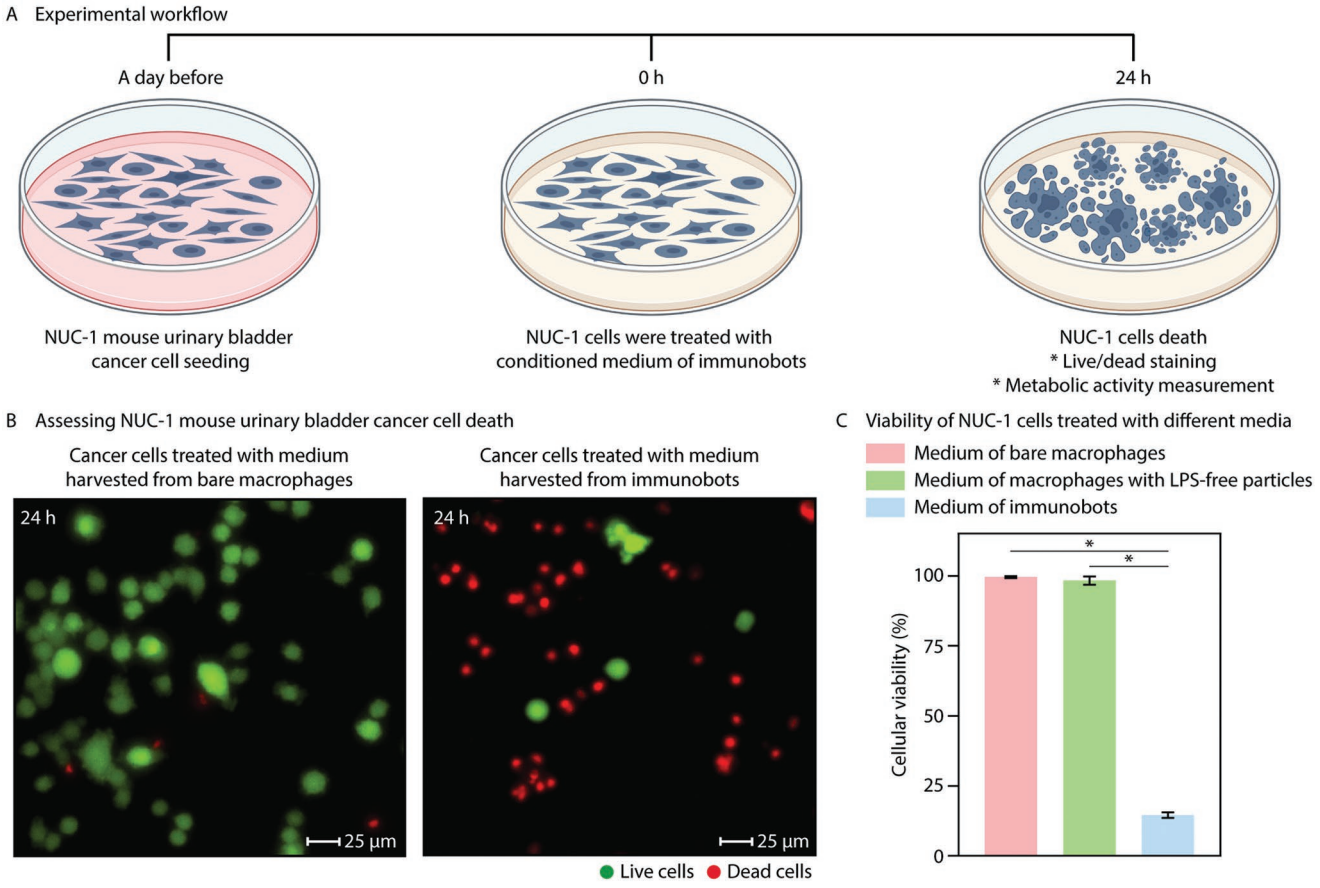



**Figure 5.** Antitumor activity of immunobots. A) Experimental workflow for analyzing antitumor activity of immunobots. The conditioned medium harvested from immunobots was transferred to NUC-1 mouse urinary bladder cancer cells, resulting in cancer cell death. B) The representative fluorescence images of NUC-1 mouse urinary bladder cancer cells stained with calcein-AM/ethidium homodimer-1 after 24 h incubation with the conditioned medium of bare macrophages and immunobots. C) The mouse urinary bladder cancer cells were treated with the conditioned medium harvested from i) bare macrophages, ii) macrophages treated with LPS-free particles, and iii) immunobots for 24 h, where the macrophages were in the M1-activation state only in the immunobots group. The viability of NUC-1 cancer cells was measured based on the quantified intracellular adenosine 5′-triphosphate (ATP) amount using the CellTiter-Glo assay after 24 h exposure to different cell culture media (*, Student's *t*-test, $p < 0.05$). Data were presented as mean ± SD, $n = 3$.

whereas F4/80 is required to induce antigen-specific efferent regulatory T cells.[33] We observed 77% of cells expressing both macrophage markers at the end of 6 d incubation period with M-CSF (Figure 6C). Additionally, we demonstrated that freshly isolated primary macrophages could sense and encapsulate foreign substances, such as magnetic decoy bacteria, where the resultant engineered cells are called *primary immunobots* (Figure 6D). We actuated and steered primary immunobots under a rotating magnetic field, and the step-out frequencies were calculated by gradually increasing the magnetic field frequency under a 10 mT rotating magnetic field and observed an average speed of 61 µm $s^{-1}$ at 30 Hz (Figure 6E,F and Movie S6, Supporting Information).

## 3. Conclusion

Here, we presented live macrophage-derived anti-tumorigenic microrobots that can be steered with remotely applied magnetic fields along assigned trajectories inside blood plasma, over a layer of endothelial cells, and against the physiologically relevant flow rates. The secreted molecules by the M1-activated immunobots into the cell culture medium can significantly inhibit the proliferation of mouse urinary bladder cancer cells in vitro. The immunobots reported in this article have a strong potential in treating solid tumors in vivo, where the immunobots can be directed towards solid tumors to recruit surrounding host immune cells to the targeted area via local pro-inflammatory cytokine secretion. Such a route has the potential to impact cellular cancer therapy. In addition, robotic navigation of live cells can impact cell-based drug delivery carriers by directing them to the action site.[34]

Despite the success achieved in in vitro tests, further improvements are still required to advance immunobots toward in vivo applications. One of the biggest challenges for the operation of immunobots in vivo is the biological barriers that immunobots should permeate from the administration to the target site for solving a targeted medical problem. The abilities of immunobots to pass through biological barriers should be investigated in detail in the ex vivo tissues and realistic


© 2022 The Authors. Small published by Wiley-VCH GmbH

16136829, 2022, 46, Downloaded from https://onlinelibrary.wiley.com/doi/10.1002/smll.202204016 by Koc University, Wiley Online Library on [15/04/2023]. See the Terms and Conditions (https://onlinelibrary.wiley.com/terms-and-conditions) on Wiley Online Library for rules of use; OA articles are governed by the applicable Creative Commons License

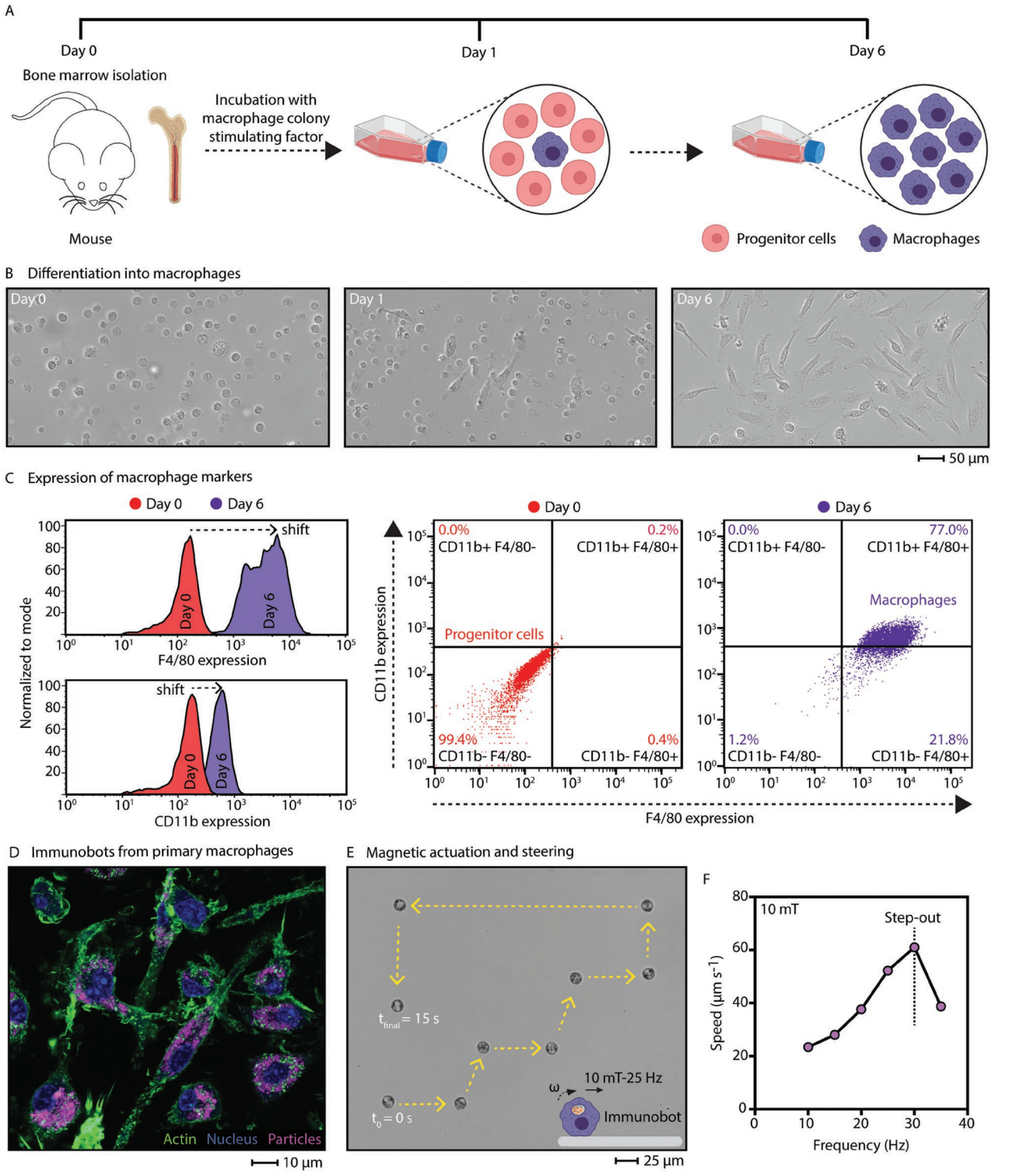



**Figure 6.** Immunobots constructed from primary macrophages. A) Progenitor cells were freshly isolated from the bone marrow of healthy mice. Incubation with macrophage colony-stimulating factor (M-CSF) for 6 d induced the differentiation of progenitor cells into macrophages. B) The DIC images illustrated the evolution of progenitor cells into macrophages over time. C) The number of progenitor cells differentiated into macrophages was assessed by flow cytometry using F4/80 and CD11b macrophage identification markers. As of day 6, the 77% of the cells had been identified as macrophages by both markers ($n = 10\,000$ events per data point). D) The internalization of magnetic decoy bacteria by primary macrophages was demonstrated through confocal microscopy by fluorescence staining of magnetic decoy bacteria, actin filaments, and the nucleus of the cells. E) Primary immunobots were capable of following a predefined trajectory under a 10 mT rotating magnetic field at 25 Hz. F) The step-out frequency of primary immunobots at a 10 mT rotating magnetic field was determined as 30 Hz with a maximum mean speed of 61 µm $s^{-1}$ by increasing the actuation frequency of the magnetic field stepwise.


© 2022 The Authors. Small published by Wiley-VCH GmbH

16136829, 2022, 46, Downloaded from https://onlinelibrary.wiley.com/doi/10.1002/smll.202204016 by Koc University, Wiley Online Library on [15/04/2023]. See the Terms and Conditions (https://onlinelibrary.wiley.com/terms-and-conditions) on Wiley Online Library for rules of use; OA articles are governed by the applicable Creative Commons License

phantoms. Moreover, depending on different body parts and local physical parameters, the immunobots may have to change their locomotion mode and propulsion speed. We have previously shown that physically engineered cells with tiny magnets maintained the crawling locomotion of macrophages, which is necessary for motion inside the tissue parenchyma.[35]

## 4. Experimental Section

*Fabrication and Characterization of FePt-Coated Silica Particles*: Silica particles (0.5 µm diameter, microParticles GmbH) were deposited on a silicon wafer treated with oxygen plasma. Activation of the wafer was essential for the uniform distribution of the silica particles, which otherwise formed inhibitive clumps. The thin coating of silica particles with FePt alloy ($L1_0$ phase, 60-nm thickness) was performed in a molecular beam epitaxy chamber under ultrahigh vacuum conditions (≈2–5 × $10^{-9}$ mbar) as described and characterized previously.[15a] The deposition of FePt is followed by an annealing step at 680 °C for 1 h. After deposition, the FePt-coated silica particles were collected in ethanol by sonication for further experiments.

SEM imaging of the FePt-coated silica particles was performed under a Zeiss Ultra 550 Gemini SEM (Carl Zeiss Inc.). The particles were spread on a glass substrate and air-dried overnight. Following air-drying, the particles were sputtered with 10 nm-thick gold using a benchtop sputter coating system (Leica EM ACE600, Leica Microsystems). SEM imaging was performed with an accelerating voltage of 3 keV and an Everhart-Thornley secondary electron detector (SE2). To conduct TEM imaging, particle solution was dropped onto a copper grid (Plano GmbH) and air-dried overnight. Imaging was performed under Philips CM 200 field emission TEM with an accelerating voltage of 200 kV. Magnetic hysteresis of the particles was characterized at the maximum uniform magnetic field of 1.8 T using a vibrating sample magnetometer (VSM) (EZ7, MicroSense (Figure S2, Supporting Information).

*Conjugation of Bacterial LPS to FePt-Coated Silica Particles*: Uncoated silica surfaces were further functionalized with bacterial LPS through a series of chemical reactions. As a first step, 3-aminopropyltriethoxysilane (APTES) was used to conjugate amino groups to the silica side of FePt-coated Janus silica particles. The FePt-coated Janus silica particles in 1 mL ethanol solution were vortexed with 50 µL APTES (Sigma-Aldrich) for 3 h. The mixture was further incubated at 65 °C for 1 h. Following centrifugation, the particles were washed multiple times with ethanol and dimethyl sulfoxide (DMSO, Sigma-Aldrich). In the second step, amino groups on particles' surfaces were modified with N-hydroxysuccinimide (NHS)–biotin by NHS–amine coupling. A solution of NHS–biotin in DMSO (5 mg $mL^{-1}$, EZ-Link NHS-Biotin, Thermo Fisher Scientific) was vortexed with the particles for 3 h. After the reaction, the particles were washed several times in DMSO and Dulbecco's phosphate buffered saline (DPBS, Gibco). In the third step, the particles were labeled with FITC-tagged streptavidin (Thermo Fisher Scientific) by using biotin-streptavidin reaction. Streptavidin solution (50 µg $mL^{-1}$ in DPBS) was vortexed with the particles for 1 h, followed by washing several times in DPBS. As the last step, biotinylated LPS from *Escherichia coli* serotype 0111:B4 (InvivoGen) was attached to particles through the biotin-streptavidin reaction. The particles were incubated with biotinylated bacterial LPS (500 µg $mL^{-1}$ in PBS) for 1 h, followed by several rounds of washing with DPBS to remove all non-bound components. Ultimately, the resultant magnetic decoy bacteria were resuspended in DPBS and sterilized under ultraviolet (UV) light for further investigations.

*Cell Culture*: Mouse peritoneal macrophage cells (J774A.1, American Type Culture Collection) were cultured in high-glucose Dulbecco's modified Eagle's medium (DMEM, Gibco) supplemented with 10% fetal bovine serum (FBS, Gibco) and 1% penicillin/streptomycin (Gibco) in a humidified, 37 °C and 5% $CO_2$ atmosphere using 75 $cm^2$ polystyrene cell culture flasks. Cells were used at passage numbers less than 10, and detachment was performed using a cell scraper upon reaching 80% confluency.

HUVECs (Lonza) were cultured in Endothelial Cell Growth Medium-2 (EBM-2, Lonza) supplemented with EGM-2 SingleQuots (Lonza) in a humidified, 37 °C and 5% $CO_2$ atmosphere using 75-$cm^2$ polystyrene cell culture flasks. Cells were used at passage numbers less than 10, and detachment was performed using trypsin (0.25 wt%)/ethylenediaminetetraacetic acid (EDTA) solution (Gibco) upon reaching 70% confluency.

Mouse urinary bladder cancer cells (NUC-1, DSMZ) were cultured in 45% Ham's F10 (Gibco), 45% DMEM (Gibco) supplemented with 10% FBS (Gibco), 1% penicillin/streptomycin (Gibco), 5 µg $mL^{-1}$ human insulin (Sigma-Aldrich), 5 µg $mL^{-1}$ human transferrin (Sigma-Aldrich), $50 \times 10^{-9}$ M hydrocortisone (Sigma-Aldrich), 5 ng $mL^{-1}$ selenite (Sigma-Aldrich), and $10 \times 10^{-6}$ M HEPES (Gibco) in a humidified, 37 °C and 5% $CO_2$ atmosphere using 75-$cm^2$ polystyrene cell culture flasks. Cells were used at passage numbers less than 10, and detachment was performed using trypsin (0.25 wt%)/EDTA solution (Gibco) upon reaching 70% confluency.

*Preparation and Characterization of Immunobots*: The J774A.1 mouse peritoneal macrophage cells were seeded on a plate the day before the experiment. The following day, cells were incubated with magnetic decoy bacteria (0.05 mg $mL^{-1}$ in DMEM). Phagocytosis of magnetic decoy bacteria was acquired time-lapse using the bright-field mode of confocal microscopy (Leica SP8) equipped with an environmental chamber to maintain physiological conditions. The prepared immunobots, after overnight incubation with magnetic decoy bacteria, were rinsed with DPBS and immediately analyzed using a Nikon Eclipse Ti-E inverted optical microscope.

For confocal images, the immunobots were fixed with 4% (v/v) paraformaldehyde (PFA, Alfa Aesar) in DPBS for 20 min and permeabilized with 0.1% (v/v) Triton X-100 (Sigma-Aldrich) in DPBS for 15 min. To stain cells, we added an aqueous solution of Hoechst 33342 (1 µg $mL^{-1}$, Thermo Fisher Scientific) and ActinRed 555 ReadyProbes (2 drops $mL^{-1}$, Life Technologies) to DPBS and incubated this solution with cells for 30 min in the dark. The Z-stack images were acquired using confocal microscopy (Leica SP8).

For SEM imaging, immunobots were fixed with 4% (v/v) PFA in DPBS for 20 min and then dehydrated for 10 min with increasing ethanol concentrations (30%, 50%, 75%, 90%, and 100%). The cells were subsequently chemically dehydrated for 10 min using increasing concentrations of hexamethyldisilazane (HMDS, Sigma-Aldrich) solutions in ethanol (33%, 50%, 67%, and 100% HMDS). The samples were thoroughly air-dried under a fume hood overnight. After air-drying, the samples were sputtered with 10 nm gold using a benchtop sputter coating system (Leica EM ACE600, Leica Microsystems). Imaging was performed under a Zeiss Ultra 550 Gemini SEM (Carl Zeiss Inc.) with an accelerating voltage of 3 keV and an SE2 detector. Pseudocolored images were created using Adobe Photoshop Software (version 21.0).

A quantitative evaluation of immunobot populations was conducted with flow cytometry (BD LSRFortessa X-20, BD Biosciences). The experiment was performed by comparing bare macrophages and macrophages incubated overnight with FITC-tagged magnetic decoy bacteria. All groups were detached from the surface and fixed with PFA (4% (v/v) in DPBS) for 20 min. After rinsing with DPBS, the cells were investigated by size (FSC) to exclude non-internalized magnetic decoy bacteria, then characterized using a blue laser (Ex/Em: 488/525 nm) to detect FITC-expressing macrophages. The data were further analyzed with FlowJo 10.8.1 software using a total of 10 000 events collected per group.

*Biocompatibility of Magnetic Decoy Bacteria*: A black/clear bottom 96-well plate (Corning) was seeded with J774A.1 cells in triplicate at a concentration of $1 \times 10^4$ cells/well the day before the experiment to allow attachment of cells. Next, the cells were treated with magnetic decoy bacteria (0.05 mg $mL^{-1}$ in DMEM) in triplicate for different time points. Following incubation for 24–72 h, the amount of ATP in the cells was measured using CellTiter-Glo assay (Promega), according to the supplier's instructions. The luminescence of the cell lysates was measured using a microplate reader (BioTek Synergy 2). To provide visual evidence, a parallel set of J774A.1 cells were stained in Live/Dead


© 2022 The Authors. Small published by Wiley-VCH GmbH

16136829, 2022, 46, Downloaded from https://onlinelibrary.wiley.com/doi/10.1002/smll.202204016 by Koc University, Wiley Online Library on [15/04/2023]. See the Terms and Conditions (https://onlinelibrary.wiley.com/terms-and-conditions) on Wiley Online Library for rules of use; OA articles are governed by the applicable Creative Commons License

Cell Imaging Kit (Invitrogen) as specified by the vendor. Images of live (calcein-AM) (Ex/Em: 488/520 nm) and dead (ethidium homodimer-1) (Ex/Em: 528/617 nm) cells were obtained using a fluorescent microscope (Nikon Eclipse Ti-E).

*Isolation of Plasma from Whole Blood*: Whole blood of freshly sacrificed C57BL/6 mouse was obtained from Einrichtung für Tierschutz, Tierärztlichen Dienst und Labortierkunde, Eberhard Karls Universität Tübingen and placed in EDTA-treated tubes. Plasma was isolated from whole blood by centrifugation at 800× *g* for 20 min at 15 °C. A two-phase mixture was obtained after centrifugation, where the supernatant was regarded as blood plasma and was immediately transferred into a clean microcentrifuge tube.

*Magnetic Actuation and Steering of Immunobots*: Immunobots were actuated and steered using a custom-made five-coiled electromagnetic setup mounted on an inverted microscope (Zeiss Axio Observer A1), as previously described.[36] The immunobots were steered under a constant 10 mT rotating magnetic field at 20 Hz in different conditions: i) on a glass substrate in a cell culture medium, ii) on a glass substrate in blood plasma, and iii) on an endothelial layer in cell culture medium. The step-out frequencies of immunobots were determined under a 10 mT rotating magnetic field by gradually increasing the frequency. An in-house MATLAB code was used to compute the mean speeds of immunobots.

*Magnetic Actuation and Steering of Immunobots against Flow*: Flow experiments were conducted in a closed microchannel (75 µm height, 3 mm width, and 12 mm length), consisting of a glass bottom piece, a double-sided tape defining channel shape and dimensions, and a poly(methyl methacrylate) (PMMA) top part encompassing fluid connections. A $CO_2$ laser cutting system (Epilog Laser, Scottsdale, AZ) was used to manufacture the desired channel shape in the double-sided tape and fluidic connections in the PMMA top piece.

The immunobots mixed in DPBS (Gibco) were loaded into syringes and introduced into the microfluidic channels through a tubing (Cole-Parmer) with an inner and outer diameter of 0.25 and 0.76 mm, respectively. The flow rates of immunobots were controlled using a syringe pump (KD Scientific Inc.). The volume flow rates of 4 and 6 µL $min^{-1}$ in the syringe pump resulted in the average flow rates of 2 and 4 mm $s^{-1}$. The motion of immunobots under flow conditions was controlled using a custom-made five-coiled electromagnetic setup under a 10 mT rotating magnetic field at 30 Hz. The real-time videos were recorded with an inverted microscope (Zeiss Axio Observer A1).

*Cellular Viability after Magnetic Actuation and Steering*: After performing magnetic actuation and steering of immunobots in static conditions under a 10 mT rotating magnetic field at 30 Hz for 5 min, the cells were incubated in a humidified 37 °C and 5% $CO_2$ atmosphere overnight. After overnight incubation, the cells were stained with a Live/Dead Cell Imaging Kit (Invitrogen) and imaged under fluorescent optical microscopy (Nikon Eclipse Ti-E). The percentage viabilities were calculated using live/dead cell counts based on Fiji software.

*Measurement of Cytokine Secretion*: To characterize the activation state of immunobots, IL-12 p40, TNF-$\alpha$, IL-6, and IL-10 secretion amounts were measured. The cell culture media were harvested from i) bare macrophages, ii) macrophages treated with LPS-free particles, and iii) immunobots at 24, 48, and 72 h. The amount of the secreted IL-12 p40 by macrophages was measured using a mouse IL-12 p40 ELISA set (BD Biosciences) by following the supplier's instructions. The optical densities were measured using a microplate reader (BioTek Synergy 2). The amount of secreted TNF-$\alpha$, IL-6, and IL-10 cytokines by macrophages was measured using BD Cytometric Bead Array (CBA) Mouse Inflammation Kit (BD Biosciences) by following the supplier's instructions. Up to 10 000 events were collected from all samples using a flow cytometer (BD LSRFortessa X-20, BD Biosciences), and the data were further analyzed with FlowJo 10.8.1 software.

*Surface and Intracellular Antibody Staining*: The features of the antibodies used in flow cytometry experiments are provided in Table S1 (Supporting Information). Cell-surface CD80 antibody staining was performed on three groups: bare macrophages, macrophages treated with LPS-free particles, and immunobots. The groups were first detached from the surface, centrifuged, and resuspended in an antibody mixture at 4 °C for 30 min in the dark. The cells were then rinsed three times before being stored in a staining buffer for further flow cytometry analysis.

For intracellular cell staining with nitric oxide synthase (iNOS) and arginase-1 (Arg-1), an intracellular fixation and permeabilization buffer set was used (Thermo Fischer Scientific). The cells were detached from the surface, incubated with fixation buffer for 20 min, and washed with staining buffer twice. The cells were then incubated with permeabilization buffer for 15 min and washed with staining buffer. The permeabilization process was repeated twice. Next, intracellular staining of cells was performed with iNOS and Arg-1 at 4 °C for 30 min in the dark. The cells were washed three times and stored in a staining buffer for flow cytometry analysis.

After the surface and intracellular antibody staining, all samples were analyzed using a flow cytometer (BD LSRFortessa X-20, BD Biosciences). Up to 10 000 events were collected from all samples, and the data were further analyzed with FlowJo 10.8.1 software.

*Assessment of Cancer Cell Death*: To investigate the antitumor activity of immunobots, the mouse urinary bladder cancer cells (NUC-1, DSMZ) ($1 \times 10^4$ cells/per well) were seeded on a black/clear bottom 96-well plate (Corning) in triplicates 1 d before the experiment. After overnight incubation, the supernatants harvested from i) bare macrophages, ii) macrophages treated with LPS-free particles, and iii) immunobots at 24 h were incubated with cancer cells (50% fresh cancer cell culture medium/50% harvested conditioned media), where the resultant macrophage: NUC-1 cell ratio was equal to 1:1 for each group. After 24 of incubation of cancer cells with different culture media, the NUC-1 cells were stained with a Live/Dead Cell Imaging Kit (Invitrogen) as specified by the supplier. Images of live (calcein-AM) (Ex/Em: 488/520 nm) and dead (ethidium homodimer-1) (Ex/Em: 528/617 nm) cells were obtained using a fluorescent microscope (Nikon Eclipse Ti-E). The amount of ATP in the NUC-1 cells was also measured using the CellTiter-Glo assay (Promega), according to the supplier's instructions. The luminescence was measured using a microplate reader (BioTek Synergy 2). The cell viability percentages for each group were calculated based on the untreated group in which the cell viability was accepted as 100%.

*Isolation and Characterization of Primary Macrophages*: Femur and tibia were obtained from freshly euthanized C57BL/6 mice from Einrichtung für Tierschutz, Tierärztlichen Dienst und Labortierkunde, Eberhard Karls University Tübingen as an animal side product (registration number: DE 08 111 1008 21). The permit and registration number for the scientific use of animal side products were issued by the office for public order, in particular, the authorities for official food control, consumer protection, and veterinary services of the state capital Stuttgart. As requested by the permit, an official holding register of the biomaterial is kept, and the used animal side products are pressure sterilized following the experiment. Bone marrow preparation and differentiation into bone marrow macrophages were performed according to published procedures.[37] Excess muscle tissue was removed from the femur and tibia; bones were rinsed in the cold, sterile DPBS (Gibco) and cut proximal to the joints. Next, bones were flushed with DPBS using a 25G needle. Cells were washed, counted, and resuspended in DMEM (Gibco) containing 10% FBS (Gibco), 1% penicillin/streptomycin (Gibco), and 2 ng $mL^{-1}$ recombinant mouse colony-stimulating factor (M-CSF, Abcam). For differentiation into bone marrow macrophages, the cells were seeded into six-well plates at a concentration of $5 \times 10^6$/well and cultured at 37 °C and 5% $CO_2$ for 6 d with an additional feeding of the cells with M-CSF containing medium on day 3.

The differentiation of progenitor cells to macrophages was analyzed using CD11b and F4/80 staining (Table S1, Supporting Information). After collecting the cells on days 0 and 6, they were centrifuged and resuspended in antibody mixtures at the concentrations suggested by the supplier at 4 °C for 30 min in the dark. Incubation for 30 min was followed by three rinses, and the expression of markers was analyzed using a flow cytometer (BD LSRFortessa X-20, BD Biosciences). Up to 10 000 events were collected from all samples, and the data were further analyzed with FlowJo 10.8.1 software.

*Statistical Analysis*: All measurements were performed with at least three replicates for each group. All quantitative values were presented as means ± standard deviation (SD) of the mean. The Student's *t*-test


© 2022 The Authors. Small published by Wiley-VCH GmbH

16136829, 2022, 46, Downloaded from https://onlinelibrary.wiley.com/doi/10.1002/smll.202204016 by Koc University, Wiley Online Library on [15/04/2023]. See the Terms and Conditions (https://onlinelibrary.wiley.com/terms-and-conditions) on Wiley Online Library for rules of use; OA articles are governed by the applicable Creative Commons License

was used for statistical analysis, and a *p*-value of less than 0.05 was considered statistically significant.

## Supporting Information

Supporting Information is available from the Wiley Online Library or from the author.

## Acknowledgements

This study was funded by the Max Planck Society. Cell cartoons were created with BioRender.com. The authors thank A. Shiva for VSM measurements and TEM analysis.

Open access funding enabled and organized by Projekt DEAL.

## Conflict of Interest

The authors declare no conflict of interest.

## Author Contributions

N.O.D., H.C., and M.S. proposed and designed the research. H.C. and M.S. supervised the research. E.S. and G.R. contributed to the FePt deposition. N.O.D. performed the preparation, characterization, magnetic actuation, and steering of immunobots. N.O.D. and D.S. performed the antibody staining, flow cytometry analysis, and enzyme-linked immunosorbent assay. N.O.D. performed experiments on the antitumor activities of immunobots. A.A. and I.C.Y. assisted with discussions and experimental procedures. A.-M.W. contributed to the experiments with the isolation of bone marrow-derived macrophages. N.O.C. led the manuscript preparation with contributions from all authors.

## Data Availability Statement

The data that support the findings of this study are available on request from the corresponding author. The data are not publicly available due to privacy or ethical restrictions.

## Keywords

cancer immunotherapy, cell-based microrobots, immune cells, immunomodulation, macrophages

Received: June 29, 2022
Revised: September 8, 2022
Published online: October 6, 2022

[1] a) H. Ceylan, J. Giltinan, K. Kozielski, M. Sitti, *Lab Chip* **2017**, *17*, 1705; b) B. J. Nelson, I. K. Kaliakatsos, J. J. Abbott, *Annu. Rev. Biomed. Eng.* **2010**, *12*, 55; c) M. Sitti, *Mobile Microrobotics*, MIT Press, Cambridge, MA **2017**; d) M. Sitti, H. Ceylan, W. Hu, J. Giltinan, M. Turan, S. Yim, E. Diller, *Proc. IEEE* **2015**, *103*, 205.

[2] a) Y. Alapan, O. Yasa, B. Yigit, I. C. Yasa, P. Erkoc, M. Sitti, *Annu. Rev. Control, Rob., Auton. Syst.* **2019**, *2*, 205; b) P. Erkoc, I. C. Yasa, H. Ceylan, O. Yasa, Y. Alapan, M. Sitti, *Adv. Ther.* **2019**, *2*, 1800064.

[3] a) V. D. Nguyen, H.-K. Min, H. Y. Kim, J. Han, Y. H. Choi, C.-S. Kim, J.-O. Park, E. Choi, *ACS Nano* **2021**, *15*, 8492; b) H. Zhang, Z. Li, C. Gao, X. Fan, Y. Pang, T. Li, Z. Wu, H. Xie, Q. He, *Sci. Rob.* **2021**, *6*, eaaz9519.

[4] C.-H. Lee, E. Y. Choi, *Int. J. Rheum. Dis.* **2018**, *25*, 11.

[5] H. Ceylan, N. O. Dogan, I. C. Yasa, M. N. Musaoglu, Z. U. Kulali, M. Sitti, *Sci. Adv.* **2021**, *7*, eabh0273.

[6] a) H. Ceylan, I. C. Yasa, U. Kilic, W. Hu, M. Sitti, *Prog. Biomed. Eng.* **2019**, *1*, 012002; b) H. Lu, T. Hoshiba, N. Kawazoe, G. Chen, *Biomaterials* **2011**, *32*, 2489.

[7] L. L. W. Wang, M. E. Janes, N. Kumbhojkar, N. Kapate, J. R. Clegg, S. Prakash, M. K. Heavey, Z. Zhao, A. C. Anselmo, S. Mitragotri, *Bioeng. Transl. Med.* **2021**, *6*, e10214.

[8] a) N. R. Anderson, N. G. Minutolo, S. Gill, M. Klichinsky, *Cancer Res.* **2021**, *81*, 1201; b) Y. Chen, Z. Yu, X. Tan, H. Jiang, Z. Xu, Y. Fang, D. Han, W. Hong, W. Wei, J. Tu, *Biomed. Pharmacother.* **2021**, *139*, 111605; c) C. Sloas, S. Gill, M. Klichinsky, *Front Immunol.* **2021**, *12*, 783305.

[9] a) A. Das, M. Sinha, S. Datta, M. Abas, S. Chaffee, C. K. Sen, S. Roy, *Am. J. Pathol.* **2015**, *185*, 2596; b) T. A. Wynn, A. Chawla, J. W. Pollard, *Nature* **2013**, *496*, 445.

[10] M. Orecchioni, Y. Ghosheh, A. B. Pramod, K. Ley, *Front. Immunol.* **2019**, *10*, 1084.

[11] A. Mantovani, S. Sozzani, M. Locati, P. Allavena, A. Sica, *Trends Immunol.* **2002**, *23*, 549.

[12] L. Suarez-Lopez, G. Sriram, Y. W. Kong, S. Morandell, K. A. Merrick, Y. Hernandez, K. M. Haigis, M. B. Yaffe, *Proc. Natl. Acad. Sci. USA* **2018**, *115*, E4236.

[13] a) M. Matsuura, *Front. Immunol.* **2013**, *4*, 109; b) F. Meng, C. A. Lowell, *J. Exp. Med.* **1997**, *185*, 1661.

[14] E. Uribe-Querol, C. Rosales, *Front. Immunol.* **2020**, *11*, 1066.

[15] a) U. Bozuyuk, E. Suadiye, A. Aghakhani, N. O. Dogan, J. Lazovic, M. E. Tiryaki, M. Schneider, A. C. Karacakol, S. O. Demir, G. Richter, M. Sitti, *Adv. Funct. Mater.* **2022**, *32*, 2109741; b) Y. Alapan, U. Bozuyuk, P. Erkoc, A. C. Karacakol, M. Sitti, *Sci. Rob.* **2020**, *5*, eaba5726.

[16] U. Bozuyuk, Y. Alapan, A. Aghakhani, M. Yunusa, M. Sitti, *Proc. Natl. Acad. Sci. USA* **2021**, *118*, 1.

[17] F. L. Miles, J. E. Lynch, R. A. Sikes, *J. Microbiol. Methods* **2015**, *2*, e29.

[18] H. Zhou, C. C. Mayorga-Martinez, S. Pané, L. Zhang, M. Pumera, *Chem. Rev.* **2021**, *121*, 4999.

[19] A. W. Mahoney, N. D. Nelson, K. E. Peyer, B. J. Nelson, J. J. Abbott, *Appl. Phys. Lett.* **2014**, *104*, 144101.

[20] I. Kocherova, A. Bryja, P. Mozdziak, A. Angelova Volponi, M. Dyszkiewicz-Konwińska, H. Piotrowska-Kempisty, P. Antosik, D. Bukowska, M. Bruska, D. Iżycki, *J. Clin. Med.* **2019**, *8*, 1602.

[21] a) A. Viola, F. Munari, R. Sánchez-Rodríguez, T. Scolaro, A. Castegna, *Front Immunol* **2019**, *10*, 1462; b) Z. Duan, Y. Luo, *Signal Transduction Targeted Ther.* **2021**, *6*, 127.

[22] R. Kamada, F. Tano, F. Kudoh, N. Kimura, Y. Chuman, A. Osawa, K. Namba, K. Tanino, K. Sakaguchi, *PLoS One* **2016**, *11*, e0160625.

[23] G. Arango Duque, A. Descoteaux, *Front. Immunol.* **2014**, *5*, 491.

[24] X. Wang, Y. Lin, *Acta Pharmacol. Sin.* **2008**, *29*, 1275.

[25] R. Parihar, J. Dierksheide, Y. Hu, W. E. Carson, *J. Clin. Invest.* **2002**, *110*, 983.

[26] D. T. Fisher, M. M. Appenheimer, S. S. Evans, *Semin. Immunol.* **2014**, *26*, 38.

[27] B. Mirlekar, *SAGE Open Med.* **2022**, *10*, 1.

[28] a) A. Nolan, H. Kobayashi, B. Naveed, A. Kelly, Y. Hoshino, S. Hoshino, M. R. Karulf, W. N. Rom, M. D. Weiden, J. A. Gold, *PLoS One* **2009**, *4*, e6600; b) P. Tripathi, P. Tripathi, L. Kashyap, V. Singh, *FEMS Immunol. Med. Microbiol.* **2007**, *51*, 443.

[29] S. P. Arlauckas, S. B. Garren, C. S. Garris, R. H. Kohler, J. Oh, M. J. Pittet, R. Weissleder, *Theranostics* **2018**, *8*, 5842.

[30] D. Aminin, Y. M. Wang, *Kaohsiung J. Med. Sci.* **2021**, *37*, 749.


© 2022 The Authors. Small published by Wiley-VCH GmbH

16136829, 2022, 46, Downloaded from https://onlinelibrary.wiley.com/doi/10.1002/smll.202204016 by Koc University, Wiley Online Library on [15/04/2023]. See the Terms and Conditions (https://onlinelibrary.wiley.com/terms-and-conditions) on Wiley Online Library for rules of use; OA articles are governed by the applicable Creative Commons License

[31] a) A. Engström, A. Erlandsson, D. Delbro, J. Wijkander, *Int. J. Oncol.* **2014**, *44*, 385; b) H.-C. Lin, J.-Y. Lin, *Integr. Cancer Ther.* **2016**, *15*, NP13.
[32] I. Ushach, A. Zlotnik, *J. Leukocyte Biol.* **2016**, *100*, 481.
[33] a) H.-H. Lin, D. E. Faunce, M. Stacey, A. Terajewicz, T. Nakamura, J. Zhang-Hoover, M. Kerley, M. L. Mucenski, S. Gordon, J. Stein-Streilein, *J. Exp. Med.* **2005**, *201*, 1615; b) E. E. B. Ghosn, A. A. Cassado, G. R. Govoni, T. Fukuhara, Y. Yang, D. M. Monack, K. R. Bortoluci, S. R. Almeida, L. A. Herzenberg, L. A. Herzenberg, *Proc. Natl. Acad. Sci. USA* **2010**, *107*, 2568; c) R. P. Kataru, K. Jung, C. Jang, H. Yang, R. A. Schwendener, J. E. Baik, S. H. Han, K. Alitalo, G. Y. Koh, *Blood* **2009**, *113*, 5650.
[34] Y. Du, S. Wang, M. Zhang, B. Chen, Y. Shen, *Nanoscale Res. Lett.* **2021**, *16*, 139.
[35] I. C. Yasa, H. Ceylan, U. Bozuyuk, A.-M. Wild, M. Sitti, *Sci. Rob.* **2020**, *5*, eaaz3867.
[36] I. C. Yasa, A. F. Tabak, O. Yasa, H. Ceylan, M. Sitti, *Adv. Funct. Mater.* **2019**, *29*, 1808992.
[37] X. Zhang, R. Goncalves, D. M. Mosser, *Curr. Protoc. Immunol.* **2008**, *83*, 14.1.1.


© 2022 The Authors. Small published by Wiley-VCH GmbH

16136829, 2022, 46, Downloaded from https://onlinelibrary.wiley.com/doi/10.1002/smll.202204016 by Koc University, Wiley Online Library on [15/04/2023]. See the Terms and Conditions (https://onlinelibrary.wiley.com/terms-and-conditions) on Wiley Online Library for rules of use; OA articles are governed by the applicable Creative Commons License